Strain driven transport for bone modeling at the periosteal surface

Leslie Banks-Sills [a,b,*], Per Ståhle [c], Ingrid Svensson [b], Noam Eliaz [a]

[a] School of Mechanical Engineering, The Fleischman Faculty of Engineering, Tel Aviv University, 69978 Ramat Aviv, Israel
[b] Division of Solid Mechanics, Lund University, SE22100 Lund, Sweden
[c] Materials Science, Technology and Society, Malmö Hogskola, SE20506 Malmö, Sweden

ARTICLE INFO

ABSTRACT

Bone modeling and remodeling has been the subject of extensive experimental studies. There have been several mathematical models proposed to explain the observed behavior, as well. A different approach is taken here in which the bone is treated from a macroscopic view point. In this investigation, a one-dimensional analytical model is used to shed light on the factors which play the greatest role in modeling or growth of cortical bone at the periosteal surface. It is presumed that bone growth is promoted when increased amounts of bone nutrients, such as nitric oxide synthase (NOS) or messenger molecules, such as prostaglandin E_2 (PGE$_2$), seep out to the periosteal surface of cortical bone and are absorbed by osteoblasts. The transport of the bone nutrients is assumed to be a strain controlled process. Equations for the flux of these nutrients are written for a one-dimensional model of a long bone. The obtained partial differential equation is linearized and solved analytically. Based upon the seepage of nutrients out of the bone, the effect of loading frequency, number of cycles and strain level is examined for several experiments that were found in the literature. It is seen that bone nutrient seepage is greatest on the tensile side of the bone; this location coincides with the greatest amount of bone modeling.

© 2010 Elsevier Inc. All rights reserved.

1. Introduction

Bone is an adaptive material which is capable of healing when fractured, as well as altering its shape and structure as a result of imposed strain [1–8]. The hollow cross-section of long skeletal bones is ideal for supporting compressive, bending or torsional loads. The dense exterior of the central part of a long bone is formed by cortical bone, also known as compact bone. Near the ends of these bones, areas of cancellous bone serve to transfer loads from the joint to its stronger cortical part. Cancellous bone is a more porous type of material formed by a lattice of rods and plates which are referred to as trabeculae. The modeling and remodeling processes in skeletal bone can alter either its external shape or its internal structure.

The cells involved in both processes include bone forming osteoblasts, osteocytes, lining cells and osteoclasts which are active in bone resorption. An osteocyte is formed from an osteoblast at an actively forming bone surface and then trapped within the bone matrix, while new osteoblasts are recruited to the active surface area. Lining cells are osteocytes at the surface that flatten out to cover an inactive bone surface [9]. The trapped osteocytes are embedded in the mineralized bone matrix in pores called lacunae. They are not isolated from each other but remain in contact via

slender cell processes running in small channels, canaliculi, in the bone matrix. The cell processes of the osteocytes are connected by gap junctions which form a network together with the lining cells. This network transfers cell signals when loading occurs. Since the network is adjacent to the bone marrow stroma, as well as the periosteum, new osteoblasts or osteoclasts can be recruited when loading conditions demand. There is experimental evidence in vivo showing that mechanical load can stimulate, directly or indirectly, responses from osteocytes and bone lining cells [10].

Osteocytes probably do not respond directly to mechanical strain or deformation, but instead indirectly to the extracellular flow caused by the loading. The fluid flow along cells or processes produces drag force and shear stress on the surface of the cell, and an electric potential called a streaming potential. Each of these signals may activate bone cells, although cell culture experiments suggest that cells are more sensitive to fluid forces than to an electric potential [11].

When cultured osteocytes are subjected to fluid shear stresses, they release several messengers, including prostaglandins and nitric oxide [12]. According to results from in vivo studies [13], prostaglandins, e.g. prostaglandin E_2 (PGE$_2$), stimulate osteoblast activity. In addition, nitric oxide is a strong inhibitor of bone resorption through processes which decrease the recruitment of osteoclasts [14].

It has been proposed that strain-adaptive modeling and remodeling is controlled by a tissue-level negative feedback system [15]. The strains in a bone moderate the biologic mechanisms that

* Corresponding author at: School of Mechanical Engineering, The Fleischman Faculty of Engineering, Tel Aviv University, 69978 Ramat Aviv, Israel.
E-mail address: banks@eng.tau.ac.il (L. Banks-Sills).

increase or decrease its strength. For low activity, e.g. bed rest or being under low-gravity conditions, bone tissue resorbs and for increased activity bone growth is stimulated. The most effective way to strengthen a long bone is to add bone at the periosteal surface. This will increase the second moment of area and the resistance to bending or torsional loading. Moreover, it has been observed that static loading does not cause bone modeling [2].

There have been some investigations in which bone was modeled to be a homogeneous, porous medium (see for example, [16]). In addition, there have been many studies in which fluid flow within an osteon has been examined based upon the concentric cylinder, Piekarski–Munro model [17] (see for example, [18–21]). A unit cell of an osteon in an homogenized model of a porous bone was employed by Wang et al. [22] to determine the distribution of fluid pressure across a bone in bending. Petrov and Pollack [23] considered the Piekarski–Munro model and found that both diffusion caused by a concentration gradient and stress induced fluid flow were ineffective as nutrient transport mechanisms. Knothe Tate and Niederer [24] also found that diffusion caused by a concentration gradient was insufficient for nutrient transport. But they found that convection was an efficient transport mechanism. In this investigation, another model is proposed which treats these issues differently. In fact, most of the studies related to the osteon examined the problem of nutrient transport on the mesoscale alone, whereas in this study a macroscale view is taken.

Clearly, modeling of bones is a three-dimensional process. In order to understand the directional and transient process, a one-dimensional model is proposed which may be extended to two and three-dimensions. With the one-dimensional model, analytical results are obtained and exploited to understand the factors which play the greatest role in bone modeling at the periosteal surface. It is proposed here that the modeling process is governed by changes in the chemical environment of the osteoblasts. The study focuses on transport of nutrients to the periosteal surface of the diaphysis of long bones. The analysis may equally well be applied to transport of messenger molecules. The porosity of the bone is accounted for by using effective material properties. When sufficient nutrients leak out at the periosteal surface, bone modeling is triggered. The model, when extended to two dimensions, can allow examination of the endosteal surface, as well as the Haversian systems. This is beyond the scope of the current investigation. In Section 2, the one-dimensional transport model is presented. Results are obtained for the concentration of bone nutrients within the bone as a function of time. A transient term is found which contributes significantly to the solution for physiological time scales. In addition, the seepage of these nutrients at the periosteal surface of the cortical bone is found as a function of time for different strain frequencies. Experiments carried out by other researchers are discussed in Section 3 and related to the results of the analytical model.

2. One-dimensional transport model for bone nutrients

In this section, a one-dimensional model is developed to study the transport of bone nutrients in a cross-section of the bone. Bone nutrients which are thought to cause the recruitment and/or differentiation of osteoblasts are NOS and PGE$_2$ [25]; these are considered in the analysis. Any other nutrients or ions, hormones, enzymes, cytokines and growth factors may be added to the analysis once the relevant parameters for these substances are known.

Consider a cross-section of a diaphysis of a mouse ulna in the yz-plane as shown in Fig. 1(a) [26]. For the one-dimensional model, the bone is treated as a long, solid, straight rod; its cross-section is shown in Fig. 1(b). The x-axis which is perpendicular to the cross-section is along the longitudinal direction of the bone and is not shown in Fig. 1. The y-coordinate has values $-a \leqslant y \leqslant a$. In this study, a is chosen to be the thickness of the cortical bone, the grey
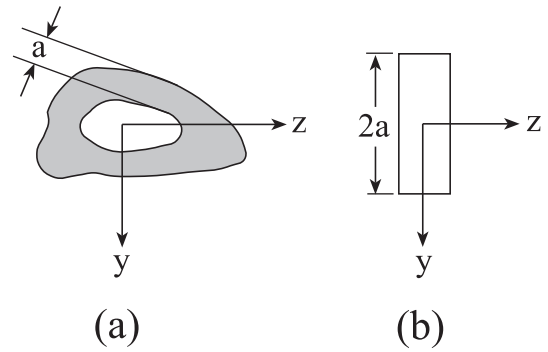

Fig. 1. Cross-section of (a) a mouse ulna [26] and (b) one-dimensional bone model.

region in Fig. 1(a). The medullary cavity is neglected. Generally, in a long bone, compressive loading takes place along its longitudinal axis (here the x-axis). As a result of its initial curvature, bending occurs. To this end, oscillating, pure, symmetric bending along the longitudinal direction of the bone is imposed. Hence, all quantities are functions of the coordinate y and time t, only. In this study, two forces are assumed to drive the diffusion of the bone nutrients. One is the change in the concentration c of the bone nutrients with position which is the basis of Fick's first law. The second is the change with position of the hydrostatic stress σ_h within the bone. For general solutes, Li [27] presented the governing equation for the flux J as:

$$J(y,t) = -Dc'(y,t) + BV_A c(y,t)\sigma_h'(y,t), \tag{1}$$

where D is the diffusion coefficient, B is the mechanical mobility, V_A is the atomic volume of bone nutrients, and the prime denotes differentiation with respect to y. Eq. (1) is applied here to the flux of bone nutrients in the bone. As a first order approximation, it is assumed that $c \approx c_0$ the initial concentration, so that:

$$J(y,t) = -Dc'(y,t) + BV_A c_0 \sigma_h'(y,t). \tag{2}$$

In Appendix A, this approximation is examined. The mechanical mobility is given by $B = D/k_B T$ [28,29] where k_B is Boltzmann's constant and T is the absolute temperature. The molar volume $\overline{V} = N_A V_A$, where N_A is Avogadro's number. Hence, Eq. (2) may be written as:

$$J(y,t) = -Dc'(y,t) + \frac{D\overline{V}c_0}{RT}\sigma_h'(y,t), \tag{3}$$

where the ideal gas constant $R = N_A k_B$.

The stress in a section of the bone is given by (Yang [30]):

$$\sigma_{xx} = E\epsilon_{xx} - \frac{E\overline{V}}{3}(c - c_0), \tag{4}$$

where E is Young's modulus and ϵ_{xx} is the axial strain. It is assumed that the bone is linear elastic, isotropic and homogeneous. It is well known that bone is anisotropic and heterogeneous. On the macroscopic level, one can assume effective material properties which allows the model to be homogeneous. Frequently, bone is assumed to be transversely isotropic; with reference to Fig. 1, the y–z plane is that of isotropy. Hence, the assumptions here for bending are reasonable. Values of E taken from the literature for actual bones are effective properties which include the porosity, as well as the fluid within the bone. It is assumed that the beam is bent in a sinusoidal manner with time. For beam bending, a kinematic assumption is made that plane sections remain plane and rotate about the neutral axis. Since y is a symmetry axis, the neutral axis is given by $y = 0$. Moreover, the sign of the moment remains unchanged during bending, so that it is possible to write:

$$\epsilon_{xx} = \frac{y\kappa_0}{2}(\cos \omega t - 1), \tag{5}$$

where κ_0 is the amplitude of the beam curvature and ω is the frequency. It may be noted that at $y = a$ (see Fig. 1), the bending strain ranges from zero to compressive values, whereas at $y = -a$, the bending strain is between zero and a tensile value. Substitution of Eq. (5) into Eq. (4) and use of

$$\sigma_h = \frac{1}{3}\sigma_{xx}, \tag{6}$$

in Eq. (3) leads to:

$$J(y,t) = -D\left(1 + \frac{E\overline{V}^2 c_0}{9RT}\right)c'(y,t) + \frac{DE\overline{V}\kappa_0 c_0}{6RT}(\cos\omega t - 1). \tag{7}$$

Fick's second law is given by

$$\dot{c}(y,t) = -J'(y,t), \tag{8}$$

where the dot above a quantity represents differentiation with respect to time. Differentiation of Eq. (7) with respect to y and substitution into Eq. (8) leads to the governing partial differential equation for the concentration, namely:

$$\lambda\dot{c}(y,t) = c''(y,t), \tag{9}$$

for $-a < y < a$, where:

$$\lambda = \frac{1}{D\left(1 + \frac{E\overline{V}^2 c_0}{9RT}\right)}. \tag{10}$$

Since all variables are anti-symmetric with respect to y (see Eq. (5)), the governing equation is solved for $0 < y < a$. The boundary condition for $y = 0$ is

$$c(0,t) = c_0, \tag{11}$$

where c_0 is the initial concentration. The characteristic flux in the body is assumed to be much larger than that which is consumed by the periosteal processes. Therefore, the flux across the periosteal boundary, here denoted as seepage, is assumed to be insignificant and without effect on the dynamic distribution of the nutrients within the bone. The seepage controls the state of the periosteum, including chemistry, physical conditions, growth rate, etc. Hence, to compute the nutrient distribution within the bone, it is assumed that the flux vanishes (it is actually very small) at the ends $|y| = a$, which by setting Eq. (7) to zero leads to:

$$ac'(a,t) = Pc_0(\cos\omega t - 1), \tag{12}$$

where a normalized nutrient driving force is defined as:

$$P \equiv \frac{D\lambda E\overline{V}\kappa_0 a}{6RT}. \tag{13}$$

The initial condition is chosen to be:

$$c(y,0) = c_0. \tag{14}$$

The governing equation, together with the boundary and initial conditions are solved by means of the Laplace transform to obtain:

$$\frac{c(y,t)}{c_0} = 1 + P\left\{\frac{2(\omega\lambda)^2}{a^2}\sum_{n=1}^{\infty}\frac{(-1)^{n+1}}{b_n^2\left[b_n^4 + (\omega\lambda)^2\right]}\sin(b_n y)e^{-\frac{b_n^2}{\lambda}t}\right.$$
$$\left. + \frac{1}{2\eta a}[A(\eta y)\sin\omega t + B(\eta y)\cos\omega t] - \frac{y}{a}\right\} \tag{15}$$

for $-a < y < a$ where

$$A(\eta y) = R(\eta a)[S(\eta a)\sinh\eta y\cos\eta y - T(\eta a)\cosh\eta y\sin\eta y], \tag{16}$$

$$B(\eta y) = R(\eta a)[S(\eta a)\cosh\eta y\sin\eta y + T(\eta a)\sinh\eta y\cos\eta y], \tag{17}$$

$$R(\eta a) = \frac{2}{\cosh 2\eta a + \cos 2\eta a}, \tag{18}$$

$$S(\eta a) = \cosh\eta a\cos\eta a + \sinh\eta a\sin\eta a, \tag{19}$$

$$T(\eta a) = \cosh\eta a\cos\eta a - \sinh\eta a\sin\eta a, \tag{20}$$

$$\eta = \sqrt{\frac{\omega\lambda}{2}}. \tag{21}$$

The parameter λ is defined in Eq. (10), and b_n is given in Eq. (46). The solution method is presented in Appendix B.

To gain an understanding of the behavior of the bone nutrients forming on the outer region of the bone which are required for modeling there, consider the nominal flux J_n across a thin layer at the boundary of the bone, e.g. the periosteum, given by

$$J_n = \frac{1}{\lambda^* h^*}\{[c(t) - c_0]|_{|y|=a} - Pc_0(\cos\omega t - 1)\}. \tag{22}$$

This expression is obtained using Eqs. (7) and (13), assuming that this layer is of thickness h^* with diffusion parameter D^* which control the release of bone nutrients at $|y| = a$. The parameter λ^* is obtained using Eq. (10) with D replaced by D^*. In Eq. (22), the first term is the concentration gradient given by $(c - c_0)/h^*$ and the second term is the strain gradient ϵ_m/h^*, where ϵ_m is the strain at $|y| = a$. The seepage S^* is found by assuming that it scales linearly with the concentration so that multiplying the nominal flux at the boundary J_n by $(c - c_0)/c_0$, one obtains:

$$S^* = \frac{1}{\lambda^* h^* c_0}([c(t) - c_0])\{[c(t) - c_0] - Pc_0(\cos\omega t - 1)\}|_{|y|=a}. \tag{23}$$

A normalized seepage may be defined as:

$$\widetilde{S} = \frac{\lambda^* h^*}{c_0}S^*. \tag{24}$$

In obtaining the results, a time averaged value of the normalized seepage is calculated as:

$$\widehat{S} = \frac{1}{t_f}\int_0^{t_f}\widetilde{S}(t)dt, \tag{25}$$

where t_f is the time during which the bone is stimulated.

3. Results

In this section, three animals are considered: a mouse, a rat and a turkey. In Table 1, approximate measurements of the thickness of the cortical bone depicted in grey in Fig. 1 and the diameter of the bones are presented. For the one-dimensional analyses, it is assumed that the half-length of the cross-section a is the thickness given in Table 1 for each animal.

The normalized concentration $c(a,t)/c_0$ and the seepage $\widetilde{S}$ are presented as a function of time. In order to plot these quantities, other physical parameters are required. The ideal gas constant $R = 8.3145$ J/(K · mol). The diffusivity coefficient D for both PGE$_2$ and NOS through the bone tissue is taken to be 6.21×10^{-10} m^2/s (see [33]). In that study dextrans were examined in bovine corti-

Table 1
Some typical measurements of bone cross-sections.

Animal/bone	Diameter (mm)	Thickness (mm)	Reference
Mouse/ulna	0.6	0.2	Lee et al. [31]
Rat/tibia	2.3	0.6	Oxlund et al. [32]
Turkey/ulna	12	1.75	Lanyon and Rubin [2]

cal bone. The value of D is taken from the cellular syncytium level. The value of c_0 is found to be approximately between 2.8×10^{-6} and 28.4×10^{-6} moles/m^3 for rats [34]. The former value was used for all animals. The volume of one mole of PGE$_2$ is found as 3.07×10^{-4} m^3 (http://www.chemspider.com/RecordView.aspx?id=10256424). The normal temperature for each of the three animals studied here is given in Table 2. Young's modulus for cortical bone in different areas of the body tends to vary. Some values are given in Table 2. These may be looked upon as approximations, but their order of magnitude is correct. It may be seen that the parameter:

$$\frac{E\overline{V}^2 c_0}{9RT}, \tag{26}$$

which appears in Eq. (10) varies between $O(10^{-7})$ and $O(10^{-8})$ for all properties appearing in this study; hence, $\lambda \sim 1/D$. Further, since the governing differential equation was linearized, it may be observed from Eq. (7) that the value of the normalized concentration c/c_0 is limited to small deviations from unity. In this study, the limiting deviation was chosen to be ±0.4.

In a study of functional adaptation of the mouse ulna [31], two different peak compressive strains of 2×10^{-3} and 3×10^{-3} were applied to the ulna of a group of mice for 10 min with a 4 Hz trapezoidal wave for 5 days/week for 2 weeks. The results showed greater positive effects on the bone formation rate in the group with the higher strain amplitude. Substituting the prescribed strain quantities into Eq. (5) leads to maximum curvature values κ_0 of 10/m and 15/m, respectively. It may be noted that the maximum strain is equal to $\kappa_0 a$. The normalized concentration in Eq. (15) was plotted at $y = \pm a$ as a function of time t. It was observed that the maximum value of the normalized concentration is too large to allow for the linearization performed in Eq. (2). Hence, this formulation may not be used for this case.

Next, consider the tests of Warden and Turner [26] on mice ulna at frequencies of 1, 5, 10, 20 and 30 Hz. For one group, 120 cycles per day were imposed on the ulna for three days with peak compressive strains ranging from about 0.0017 and 0.0025. It may be noted that the strain values varied somewhat for different frequencies with the same applied load. Loading was applied by means of a sine wave. The bone thickness was taken from Table 1 as $a = 0.2$ mm; whereas the temperature and Young's modulus were those in Table 2, namely $T = 310.5$ K and $E = 23$ GPa, respectively. It may be noted that Young's modulus in Table 2 is for mouse tibia. For the strain $\epsilon = -0.0017$ and a frequency of 1 Hz and 5 Hz, loading lasts for 120 s and 24 s, respectively, so that the concentration is too large here to allow for linearization. Only for frequencies of 10, 20 and 30 Hz with the imposed strain and the time intervals of 12, 6 and 4 s, respectively, can the model be employed. The concentration at $y = \pm a$ for each of these cases is shown in Fig. 2. It may be observed that the frequency does not affect the general trend of the concentration. At $y = a$ (the compressive side of the bone), the concentration is seen to decrease with increasing values of time. At $y = -a$ (the tensile side of the bone), the curves are reflected about $c = c_0$ so that they increase with time. It is seen at $y = a$ and $y = -a$ that the concentration deceases/increases by a maximum of about

Table 2
Temperature and Young's modulus of cortical bone of the animals studied.

Animal/bone	T (K)	E (GPa)	Reference for E
Mouse/tibia	310.5[a]	23	Somerville et al. [35]
Rat/tibia	310.5[b]	8.5	Mattila et al. [36]
Turkey/ulna	314[c]	16.95	Ricos et al. [37]

[a] http://lvma.org/mouse.html.
[b] http://research.uiowa.edu/animal/?get=rat.
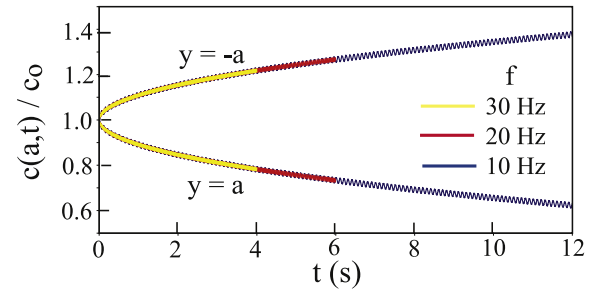[c] Tabler [38].

Fig. 2. Normalized concentration of bone nutrients for mouse ulnas at the outer edges of the bone with frequency of $f = 10$, 20 and 30 Hz and applied maximum peak compressive strain of 0.0017.

22%, 27%, and 38%, respectively for frequencies of 10, 20 and 30 Hz. For times greater than 12 s and these parameters, the linearized model cannot be employed.

These curves are typical for all of the graphs plotted in this study. It is interesting to examine the various terms in the expression for the concentration in Eq. (15). The first term represents ambient conditions. The exponential term represents the transient which at $t = 0$ balances with y/a. The former term is caused by the imposed oscillating strain in Eq. (5). For physiological time scales, this term makes a significant contribution to the concentration. As time increases, the term y/a dominates. The oscillatory term involving $\sin \omega t$ and $\cos \omega t$ causes the solution to oscillate about other dominant terms as may be observed in Fig. 2.

For each of these frequencies, the normalized seepage $\tilde{S}$ in Eq. (24) may be plotted. As an example, consider the graph in Fig. 3 for $f = 10$ Hz. In Fig. 3(a), the seepage at $y = a$ is plotted; this is on the side of the bone which is in compression. For $y = -a$, the side of the bone which is in tension, as expected much higher values of bone nutrient seepage are found. Nonetheless, even on the compressive side of the bone, bone nutrients are released. If one looks carefully at Fig. 3(a), it may be seen that each of the peaks is associated with a curve for which there is area beneath it. The area under the curves may be calculated to yield the total average seepage given in Eq. (25). For each of the frequencies examined and at each side of the bone, the results are presented in Table 3.

It was seen in Warden and Turner [26] that the larger load of 2 N is equivalent to a compressive strain of approximately 0.0025; this case could not be analyzed with the linearized model. However, a load of 1 N was considered with $\epsilon = -0.001$. Calculations showed that the concentration and seepage were considerably reduced as compared to that when $\epsilon = -0.0017$. Hence, it is seen that seepage decreases with increasing frequency (see Table 3) and increases with increasing strain. Moreover, the seepage values are one to two orders of magnitude larger on the tensile side of the bone than on the compressive side. It should be noted, however, that the number of cycles in each experiment was a constant of 120; so that, for higher frequencies, the loading time was shorter.

Rat tibiae were examined by Turner et al. [39]. Loading was applied by means of a sine wave with a frequency of 2 Hz for 18 s per day. The applied compressive strain varied from about 0.0006 to 0.002. It was seen that at or below a compressive strain of 0.00105, there was no increase in bone formation. To carry out these analyses here, the value of the bone thickness $a = 0.6$ mm was taken from Table 1. Young's modulus was taken as $E = 8.5$ GPa and $T = 310.5$ K (see Table 2). The normalized concentration in Eq. (15) is illustrated in Fig. 4 on the tensile side of the bone ($y = -a$) for four strain values. As expected, as the absolute value of the strain increases, the concentration diverges further from its ambient value c_0. Integrating the normalized seepage over the
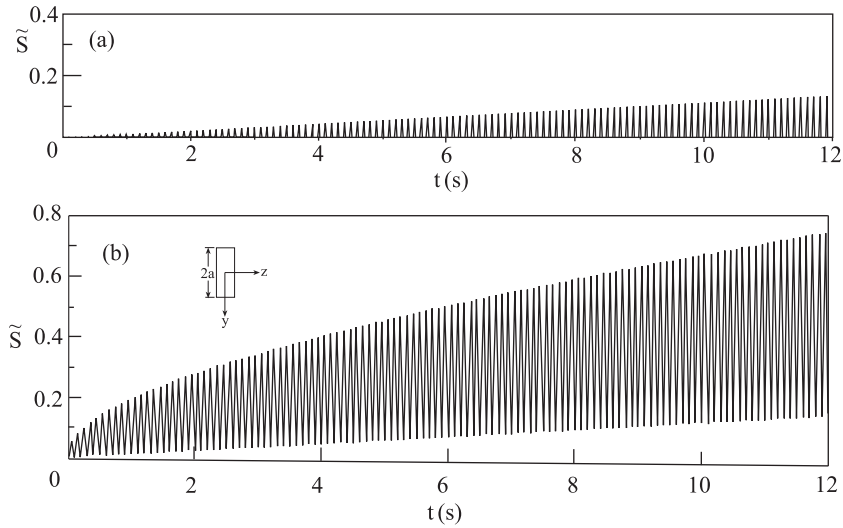
Fig. 3. Normalized seepage for mouse ulnas with frequency of f = 10 Hz and applied maximum peak compressive strain of 0.0017 at (a) $y = a$ and (b) $y = -a$.

Table 3
Time averaged, normalized seepage in Eq. (25) for the mouse ulna at a given frequency.

	f (Hz)	10	20	30
$\widehat{S}$	$y = a$	0.013	0.005	0.003
	$y = -a$	0.27	0.18	0.14

Table 4
Time averaged, normalized seepage in Eq. (25) for the rat tibia with a given compressive strain for $y = -a$.

ϵ	0.0006	0.001	0.0015	0.002
$\widehat{S}(\times 10^{-2})$	0.16	0.44	1.00	1.78

time period of 18 s as shown in Eq. (25) leads to the values presented in Table 4. It may be observed that the average seepage $\widehat{S}$ increases with strain. Apparently, a seepage level below 0.44×10^{-2} is too low to induce bone formation.

Next, in the classical isolated avian turkey ulna model [2], 100 consecutive cycles of a 1 Hz square ramped wave were applied. The strain rate during the ramp was 0.01 s^{-1}. During the rest of the day, the ulna was disused. The maximum compressive strain during loading was −0.002 in the mid-shaft of the ulna. This can be compared with the conditions during normal flapping which have been measured as ϵ_{max} = −0.0033 and a maximum strain rate of 0.056 s^{-1}. One group of turkey ulnas was loaded statically with the corresponding strain amplitude. Bones loaded dynamically showed a 24% increase in cross-sectional area, while both the group loaded statically and that unloaded showed a decrease of 13% in bone cross-sectional area. With the thickness of the bone taken as a = 1.75 mm (see Table 1), the normal temperature of the

turkey T = 314 K and Young's modulus E = 17 GPa (see Table 2), the normalized concentration in Eq. (15) was calculated and is presented in Fig. 5 at $y = -a$. Similar behavior as compared to the other cases is observed. For the largest compressive strain considered, the increase in the normalized concentration is about 18% which is within the range of the linearized model. According to Lanyon and Rubin [2], a peak compressive strain of 0.002 is sufficient to increase the bone cross-section. Thus, the seepage level determined here should be sufficient. For a strain of −0.0033 achieved by normal flapping, the seepage level is approximately three times greater, implying that greater bone growth is expected.

4. Summary and conclusions

In this study, a one-dimensional model for strain driven transport of bone nutrients was presented. The differential equation was linearized which required the concentration not to differ too
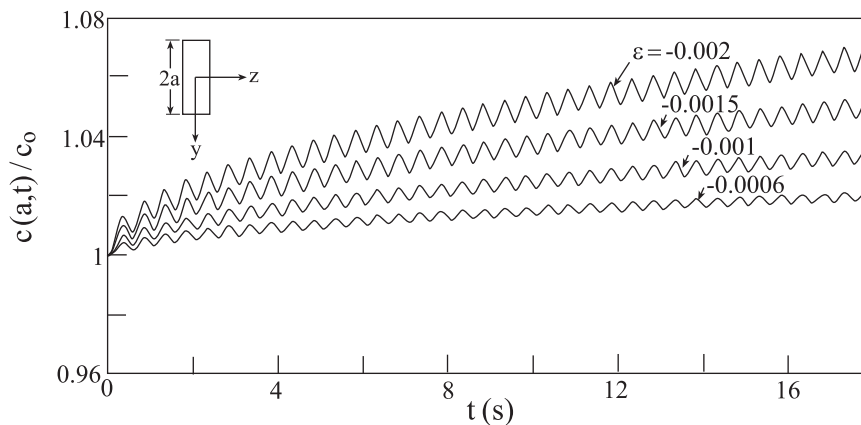

Fig. 4. Normalized concentration when $y = -a$ for rat tibias for a frequency of f = 2 Hz and applied maximum peak compressive strains of 0.0006, 0.001, 0.0015 and 0.002.
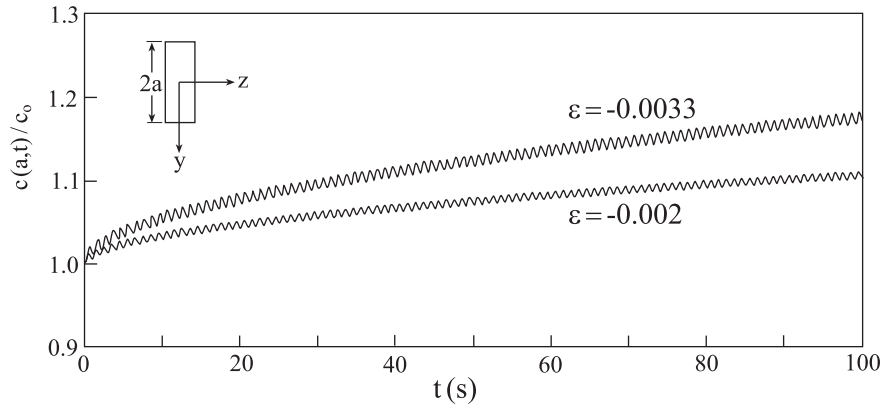
Fig. 5. Normalized concentration for turkey ulnas for a frequency of $f = 1$ Hz and applied maximum peak compressive strains of 0.002 and 0.0033 at $y = -a$.

much from its ambient value. A transient term was found which dominates the results for time scales described in many functional adaptation tests on animals. Three animals were considered: a mouse, a rat and a turkey. There have been quite a few experiments on these animals in which their limbs were loaded. The key quantities needed to evaluate the model include the frequency of loading, the peak strain levels, and the number of cycles used. In addition, various properties are required such as the diffusion coefficient of bone nutrients, their molar volume, the ambient concentration without applied load, Young's modulus of the bone, as well as its thickness, and the temperature of the animal. Indeed, it is desirable to obtain more accurate values of the diffusion coefficient, the molar volume and the ambient concentration of the bone nutrients. Tests continue to be carried out to determine the mechanical properties of different bones. In addition, two other parameters have been defined in this study which are D^* and h^*, a diffusion coefficient which governs seepage out of the bone and the distance over which this takes place. Since these two constants appear as a ratio, their ratio may be measured.

It was seen that the model predicts an increase in the divergence of the concentration from its ambient level and the average seepage of bone nutrients at the bone edge with an increase in peak strain level and number of cycles imposed. These trends seem logical. Moreover, the seepage at the tensile side of the bone was found to be one to two orders of magnitude larger than those at the compressive side. This would seem to imply that more bone growth could be expected on the side of the bone which is in tension. In fact, Mosley and Lanyon [40] found this to be the case for rat ulnas subjected to axial loads. For the mice tested by Warden and Turner [26], in which the frequency was increased but the number of cycles was held constant, the lowest frequency for which the linearization of the model could be justified showed the highest bone nutrient seepage level. This corroborates the findings in the experiments in which higher bone modeling was observed for a frequency of 10 Hz. The model could not be employed for the experiments of Lee et al. [31] on mice. The number of cycles caused the concentration to diverge considerably from its ambient value so that linearization was not justified. With the rats experimented on by Turner et al. [39], the model showed that the divergence of the bone nutrient concentration from its ambient value increased with increasing strain level. The bone nutrient seepage also increased. It was seen in the experiments that for a compressive strain level less than or equal to 0.00105, bone formation did not occur. Perhaps the model may be calibrated by this information. Finally, the turkey ulna was investigated by Lanyon and Rubin [2]. In that study, it was seen that static loading caused bone loss. The transport model presented here does not describe static loading. Perhaps a similar approach can be used to understand this phenomenon. For the dynamic loading, the seepage level increased with increasing strain. No results for bone formation were presented for $\epsilon = -0.0033$ which was measured for normal flapping. According to the model, increased bone formation should occur for this strain level as compared to the testing strain level. The simplified model presented here appears justified since it qualitatively captures the trends found for many of the basic phenomena observed in animal experimentation.

To analyze more general cases, the transport model may be extended into the nonlinear range. The differential equation in Eq. (9) may be easily reformulated. A numerical solution is required. In addition, finite element analyses in two and three dimensions may be carried out to model these problems. However, the basic behavior is elucidated by the one-dimensional model presented here. In addition, the parameters necessary for performing more complex analyses have been delineated.

Acknowledgements

Appendix A. First order approximation

In this appendix, a motivation for the first order approximation that was assumed for the concentration $c(y,t)$ is given. Inserting Eqs. (4) and (5) into Eq. (1) and using the Einstein relation for the mechanical mobility, a relation between the flux and concentration is found as:

$$J(y,t) = -Dc'(y,t) + \frac{DE\overline{V}c(y,t)}{3RT}\left[\frac{\kappa_0}{2}(\cos\omega t - 1) - \frac{\overline{V}c'(y,t)}{3}\right]. \quad (27)$$

Note that in the linearized version of Eq. (7), $c(y,t)$ was replaced by c_0. By substituting $y = a\hat{y}$ and $c = c_0\hat{c}$ into Eq. (27), one obtains:

$$\frac{a}{Dc_0}J(\hat{y},t) = -\hat{c}'(\hat{y},t) + \frac{E\overline{V}a\hat{c}(\hat{y},t)}{3RT}\left[\frac{\kappa_0}{2}(\cos\omega t - 1) - \frac{\overline{V}c_0\hat{c}'(\hat{y},t)}{3a}\right] \quad (28)$$

where the prime denotes differentiation with respect to $\hat{y}$. The following two dimensionless parameters are introduced:

$$\delta = \frac{E\overline{V}a\kappa_0}{6RT} \quad \gamma = \frac{E\overline{V}^2c_0}{9RT}, \quad (29)$$

resulting in:

$$\frac{a}{Dc_0}J(\hat{y},t) = -\hat{c}'(\hat{y},t) + \delta\hat{c}(\hat{y},t)(\cos\omega t - 1) - \gamma\hat{c}(\hat{y},t)\hat{c}'(\hat{y},t). \quad (30)$$

It may be noted that the parameters in Eq. (29) are related to the normalized nutrient driving force in Eq. (13) by

$$P = \frac{\delta}{1+\gamma}. \quad (31)$$

Differentiating Eq. (30) with respect to $\hat{y}$ and use of Eq. (8) leads to:

$$\dot{\hat{c}} = \hat{c}'' - \delta\hat{c}'(\cos\hat{\omega}\hat{t} - 1) + \gamma\hat{c}'^2 + \gamma\hat{c}\hat{c}'', \quad (32)$$

where the dot over a quantity denotes differentiation with respect to $\hat{t}$, $t = a^2\hat{t}/D$ and $\omega = D\hat{\omega}/a^2$. Eq. (32) is a dimensionless partial differential equation.

The maximum strain $a\kappa_0$ provides the only stimulus for transport and it only enters via the parameter δ. Thus, the concentration $\hat{c}$ may be expanded for small values of strain, i.e., small values of δ, as follows:

$$\hat{c}(\hat{y},\hat{t}) = 1 + \delta\hat{c}_1(\hat{y},\hat{t}) + \delta^2\hat{c}_2(\hat{y},\hat{t}) + \delta^3\hat{c}_3(\hat{y},\hat{t}) + O(\delta^4). \quad (33)$$

Substituting Eq. (33) into Eq. (32) leads to:

$$\dot{\hat{c}}_1 - (1+\gamma)\hat{c}_1'' = 0, \quad (34)$$

$$\dot{\hat{c}}_2 - (1+\gamma)\hat{c}_2'' = -\hat{c}_1'(\cos\hat{\omega}\hat{t} - 1) + \gamma(\hat{c}_1\hat{c}_1'' + \hat{c}_1'^2), \quad (35)$$

$$\dot{\hat{c}}_3 - (1+\gamma)\hat{c}_3'' = -\hat{c}_2'(\cos\hat{\omega}\hat{t} - 1) + \gamma(\hat{c}_2\hat{c}_1'' + 2\hat{c}_1'\hat{c}_2' + \hat{c}_1\hat{c}_2''). \quad (36)$$

It should be noted that the argument in Eqs. (34)–(36) is $(\hat{y},\hat{t})$. Boundary conditions at $\hat{y} = 0$ are $\hat{c}_1(0,\hat{t}) = \hat{c}_2(0,\hat{t}) = \hat{c}_3(0,\hat{t}) = 0$ and setting $J \approx 0$ in Eq. (27) at $\hat{y} = 1$ leads to the boundary conditions:

$$\hat{c}_1' = \frac{\cos\hat{\omega}\hat{t} - 1}{1+\gamma}, \quad (37)$$

$$\hat{c}_2' = \frac{\hat{c}_1(\cos\hat{\omega}\hat{t} - 1) - \gamma\hat{c}_1\hat{c}_1'}{1+\gamma}, \quad (38)$$

$$\hat{c}_3' = \frac{\hat{c}_2(\cos\hat{\omega}\hat{t} - 1) - \gamma(\hat{c}_1\hat{c}_2' + \hat{c}_2\hat{c}_1')}{1+\gamma}, \quad (39)$$

where the argument in Eqs. (37)–(39) is $(1,\hat{t})$.

The partial differential equation in (34) is identical to that in Eq. (9) with the boundary condition in Eq. (37) identical to that in Eq. (12). When solved together with the boundary condition at $\hat{y} = 0$ and the initial condition at $\hat{t} = 0$, the first order approximation to Eq. (32) is obtained. Eqs. (34)–(36) may be solved one by one using the boundary conditions (37)–(39), together with the boundary conditions at $\hat{y} = 0$ and the initial condition at $\hat{t} = 0$; in this way, higher order terms for the concentration may be obtained.

Appendix B. Solution of the partial differential equation

The governing partial differential equation in Eq. (9), the boundary conditions in Eqs. (11) and (12) and the initial condition in Eq. (14) for the concentration of bone nutrients are solved by means of the Laplace transform. The Laplace transform is defined as (see Churchill [41]):

$$C(y;s) = \int_0^\infty c(y,t)e^{-st}dt, \quad (40)$$

where s is the Laplace transform variable. The inverse transform is given by

$$c(y,t) = \frac{1}{2\pi i}\int_{\gamma-i\infty}^{\gamma+i\infty} C(y;s)e^{st}ds, \quad (41)$$

where γ is a real, positive constant, and $i = \sqrt{-1}$. Taking the Laplace transform of Eq. (9) leads to:

$$C''(y;s) - \lambda sC(y;s) = -\lambda c_0. \quad (42)$$

The initial condition in Eq. (14) has been used in the derivation of the ordinary differential equation in Eq. (42). The transform of the boundary condition in Eq. (11) is given by

$$C(0;s) = \frac{c_0}{s}, \quad (43)$$

whereas, the transform of the boundary condition in Eq. (12) is given by

$$C'(a;s) = \frac{Pc_0}{a}\left(\frac{s}{s^2+\omega^2} - \frac{1}{s}\right). \quad (44)$$

The solution to Eq. (42) with application of the boundary conditions leads to:

$$C(y;s) = \frac{c_0}{s} + \frac{Pc_0}{a}\left(\frac{s}{s^2+\omega^2} - \frac{1}{s}\right)\frac{\sinh\left(\sqrt{\lambda s}\,y\right)}{\sqrt{\lambda s}\cosh\left(\sqrt{\lambda s}\,a\right)}. \quad (45)$$

The inverse transform in Eq. (41) is applied to the solution in Eq. (45). It may be shown that the $\sqrt{s}$ is a removable singularity. Moreover, the term in parentheses has simple poles at $s = \pm i\omega$; for the second term, there is a simple pole at $s = 0$. For both terms there are simple poles at $s = -b_n^2/\lambda$ where:

$$b_n = \frac{(2n-1)\pi}{2a}, \quad (46)$$

and $n = 1,2,\ldots$. It may be noted that the integral in Eq. (41) on the part circular path far from the origin, goes to zero. Hence, the inverse transform may be evaluated by the residue theorem with the result given in Eq. (15).

References

[1] L.E. Lanyon, Functional strain as a determinant for bone remodeling, Calcif. Tissue Int. 36 (1984) S56.
[2] L.E. Lanyon, C.T. Rubin, Static vs dynamic loads as an influence on bone remodelling, J. Biomech. 17 (1984) 897.
[3] T.S. Gross, J.L. Edwards, K.J. McLeold, C.T. Rubin, Strain gradients correlate with sites of periosteal bone formation, J. Bone Miner. Res. 12 (1997) 982.
[4] S. Judex, R.F. Zernicke, High-impact exercise and growing bone: relation between high strain rates and enhanced bone formation, J. Appl. Physiol. 88 (2000) 2183.
[5] P.J. Ehrlich, L.E. Lanyon, Mechanical strain and bone cell function: a review, Osteoporos. Int. 13 (2002) 688.
[6] R.L. De Souza, M. Matsuura, F. Eckstein, S.C.F. Rawlinson, L.E. Lanyon, A.A. Pitsillides, Non-invasive axial loading of mouse tibiae increases cortical bone formation and modifies trabecular organization: a new model to study cortical and cancellous compartments in a single loaded element, Bone 37 (2005) 810.
[7] M. Isaksson, C.C. van Donkelaar, R. Huiskes, K. Ito, Corroboration of mechanoregulatory algorithms for tissue differentiation during fracture healing: comparison with in vivo results, J. Orthop. Res. 24 (2006) 898.
[8] L. Xie, J.M. Jacobson, E.S. Choi, B. Busa, L.R. Donahue, L.M. Miller, C.T. Rubin, S. Judex, Low-level mechanical vibrations can influence bone resorption and bone formation in the growing skeleton, Bone 39 (2006) 1059.
[9] E.H. Burger, J. Klein-Nulend, Mechanotransduction in bone – role of the lacuno-canalicular network, FASEB J. 13 (1999) S101.
[10] A.G. Robling, A.B. Castillo, C.H. Turner, Biomechanical and molecular regulation of bone remodeling, Annu. Rev. Biomed. Eng. 8 (2006) 455.
[11] B.R. Beck, Y-X. Qin, K.J. McLeod, M.W. Otter, On the relationship between streaming potential and strain in an in vivo bone preparation, Calcif. Tissue Int. 71 (2002) 334.
[12] E.H. Burger, J. Klein-Nulend, Responses of bone cells to mechanical forces in vitro, Adv. Dent. Res. 13 (1999) 93.
[13] W.S.S. Jee, S. Mori, X.J. Li, S. Chan, Prostaglandin E2 enhances cortical bone mass and activates intracortical bone remodelling in intact and ovariectomized female rats, Bone 11 (1990) 253.
[14] X. Fan, E. Roy, L. Zhu, T.C. Murphy, C. Ackert-Bicknell, C.M. Hart, C. Rosen, M.S. Nanes, J. Rubin, Nitric oxide regulates receptor activator of nuclear factor-κB ligand and osteoprotegerin expression in bone marrow stromal cells, Endocrinology 145 (2004) 751.
[15] H.M. Frost, A 2003 update of bone physiology and Wolff's Law for clinicians, Angle Orthod. 74 (2004) 3.
[16] R.A. Salzstein, S.R. Pollack, A.R.T. Mak, N. Petrov, Electromechanical potentials in cortical bone – I. A continuum approach, J. Biomech. 20 (1987) 261.

[17] K. Piekarski, M. Munro, Transport mechanism operating between blood supply and osteocytes in long bones, Nature 269 (1977) 80.

[18] Y. Zeng, S.C. Cowin, S. Weinbaum, A fiber matrix model for fluid flow and streaming potentials in the canaliculi of an osteon, Ann. Biomed. Eng. 22 (1994) 280.

[19] M.L. Knothe Tate, U. Knothe, An ex vivo model to study transport processes and fluid flow in loaded bone, J. Biomech. 33 (2000) 247.

[20] L. Wang, S.C. Cowin, S. Weinbaum, S.P. Fritton, Modeling tracer transport in an osteon under cyclic loading, Ann. Biomed. Eng. 28 (2000) 1200.

[21] M.L. Knothe Tate, Mixing mechanisms and net solute transport in bone, Ann. Biomed. Eng. 29 (2001) 810.

[22] L. Wang, S.P. Fritton, S.C. Cowin, S. Weinbaum, Fluid pressure relaxation depends upon osteonal microstructure: modeling an oscillatory bending experiment, J. Biomech. 32 (1999) 663.

[23] N. Petrov, S.R. Pollack, Comparative analysis of diffusive and stress induced nutrient transport efficiency in the lacunar–canalicular system of osteons, Biorheology 40 (2003) 347.

[24] M.L. Knothe Tate, P. Niederer, A theoretical FE-based model developed to predict the relative contribution of convective and diffusive transport mechanisms for the maintenance of local equilibria within cortical bone, Adv. Heat Mass Transf. Biotechnol. 40 (1998) 133.

[25] C.H. Turner, R.M. Pavalko, Mechanotransduction and functional response of the skeleton to physical stress: the mechanisms and mechanics of bone adaption, J. Orthop. Sci. 3 (1998) 346.

[26] S.J. Warden, C.H. Turner, Mechanotransduction in cortical bone is most efficient at loading frequencies of 5–10 Hz, Bone 34 (2004) 261.

[27] J.C.M. Li, Physical chemistry of some microstructural phenomena, Metall. Mater. Trans. A 9 (1978) 1353.

[28] A. Einstein, The motion of elements suspended in static liquids as claimed in the molecular kinetic theory of heat, Ann. Phys. Leipzig 17 (1905) 549.

[29] Y. Fukai, The Metal-Hydrogen System: Basic Bulk Properties, Springer-Verlag, Berlin, 1993. p. 208.

[30] R. Yang, Interaction between diffusion and chemical stresses, Mater. Sci. Eng. A 409 (2005) 153.

[31] K.C.L. Lee, A. Maxwell, L.E. Lanyon, Validation of a technique for studying functional adaptation of the mouse ulna in response to mechanical loading, Bone 31 (2002) 407.

[32] B.S. Oxlund, G. Örtoft, T.T. Andreasson, H. Oxlund, Low-intensity, high-frequency vibration appears to prevent the decrease in strength of the femur and tibia associated with ovariectomy of adult rats, Bone 32 (2003) 69.

[33] R.B. Patel, J.M. O'Leary, S.J. Bhatt, A. Vasanja, M.L. Knothe Tate, Determining the permeablility of cortical bone at multiple length scales using fluorescence recovery after photobleaching techniques, in: Proceedings of the 51st Annual Meeting of the Orthopaedic Research Society, Washington, DC, 2005, (Paper No. 0141).

[34] C. Miyaura, M. Inada, C. Matsumoto, T. Ohshiba, U. Naonori, T. Shimizu, A. Ito, An essential role of cytosolic phospholipase A2α in prostaglandin E2-mediated bone resorption associated with inflammation, J. Exp. Med. 197 (2003) 1303.

[35] J.M. Somerville, R.M. Aspden, K.E. Armour, K.J. Armour, D.M. Reid, Growth of C57B1/6 mice and the material and mechanical properties of cortical bone from the tibia, Calcif. Tissue Int. 74 (2004) 469.

[36] P. Mattila, M. Knuuttila, V. Kovanen, M. Svanberg, Improved bone biomechanical properties in rats after oral xylitol administration, Calcif. Tissue Int. 64 (1999) 340.

[37] V. Ricos, D.R. Pedersen, T.D. Brown, R.B. Ashman, C.T. Rubin, R.A. Brand, Effects of anisotropy and material axis registration on computed stress and strain distributions in the turkey ulna, J. Biomech. 29 (1996) 261.

[38] G.T. Tabler, The challenges facing turkey growers, Avian Advice 6 (2004). <http://www.thepoultrysite.com/articles/264/the-challenges-facing-turkey-growers>.

[39] C.H. Turner, M.R. Forwood, J-Y. Rho, T. Yoshikawa, Mechanical loading thresholds for lamellar and woven bone formation, J. Bone Miner. Res. 9 (1994) 87.

[40] J.R. Mosley, L.E. Lanyon, Strain rate as a controlling influence on adaptive modeling in response to dynamic loading of the ulna in growing male rats, Bone 23 (1998) 313.

[41] R.V. Churchill, Operational Mathematics, McGraw Hill, New York, 1958.